J. Fluid Mech. (1991), *vol.* 223, *pp.* 57–81
Printed in Great Britain

The effect of the contact line on droplet spreading

By PATRICK J. HALEY AND MICHAEL J. MIKSIS
Department of Engineering Sciences and Applied Mathematics, Northwestern University, Evanston, IL 60208, USA

(Received 18 January 1990)

The motion of the free surface of a viscous droplet is investigated. By using lubrication theory a model is developed for the motion of the free surface which includes both the effect of slip and the dependence of the contact angle on the slip velocity. We solve the resulting nonlinear partial differential equation in several ways. First we investigate the initial motion of the drop at a non-equilibrium contact angle using the method of matched asymptotics. Then we develop a pseudo-spectral method to numerically solve the full nonlinear system. The dependence of the spreading rate of the drop on the various physical parameters and for different slip models is determined.

1. Introduction

The motion of a drop on a solid surface is a moving-boundary problem in fluid mechanics of considerable interest and difficulty. Besides the obvious difficulties associated with any moving interface, the behaviour of the fluid in the neighbourhood of the contact line (three-phase line) presents an added complication. The contact line is the curve formed when an interface between two immiscible fluids (e.g. air and water) intersects a solid. The diffieulty is as much a modelling problem as an analytical one associated with the solution of the equations of motion. First the no-slip condition, which is normally used at the boundary between a solid and a liquid, introduces a non-integrable force singularity at the contact line. Therefore this condition has to be modified. Second, the behaviour of the contact angle has been found experimentally to be a complicated function of the contact-line speed. Therefore this functional relationship has to be somehow included in any analysis of the moving-boundary problem. Both of these points have been addressed by several authors (see e.g. Dussan V. 1979; Davis 1983; and de Gennes 1985 for a review). Here we shall carefully study a lubrication model of droplet motion which overcomes the above difficulties. Our aim is to show explicitly how the different physical parameters and different models of the slip behaviour at the contact line affect the spreading rate of the droplet. The solution of the model will be determined analytically in several limiting cases. Also we solve the model equations numerically by using a pseudo-spectral method.

Many experiments have been done to determine the relationship between the contact angle and the contact-line speed (e.g. Hoffman 1975; Johnson, Dettre & Brandeth 1977; Dussan V. 1979; and Chen 1988). These show that the contact-line speed, U_S, is a monotonic increasing function of the contact angle, Θ. The experiments indicate that a range of angles $[\Theta_R, \Theta_A]$, exists for which U_S is zero, a phenomenon known as contact-angle hysteresis. This implies that there will be a very complicated nonlinear motion of the droplet. In particular any model of the droplet motion should reflect this complicated behaviour of the contact line. This is usually

done by giving a boundary condition at the contact line which relates the contact angle to the slip velocity of the contact line. Because of the difficulty in solving such a boundary-value problem several analytical attempts to solve for the interface motion of droplet (Greenspan 1978; Davis 1980) have used a linear relation between Θ and U_S. This greatly simplifies the analysis and allows analytical solutions in several limiting cases. These calculations give reasonable results if we assume that $\Theta_A \approx \Theta_R$. Recently Young & Davis (1987) have allowed for contact-angle hysteresis in their study of a plate oscillating across a liquid interface. By considering the low-capillary-number limit they were able to reduce the problem to the solution of a second-order ordinary differential equation which included the contact-angle hysteresis. Also recently the non-isothermal spreading of liquid drops with a contact line has been considered by Ehrhard & Davis (1990). Their analysis was for small capillary numbers but allowed different contact angle *vs.* slip velocity relationships. Here we shall consider linear, piecewise quadratic and cubic contact angle *vs.* slip velocity relationships.

Although the no-slip condition is the accepted boundary condition between a fluid and a solid, it can lead to complications in systems with moving contact lines. In analysing the fluid motion near a moving contact line, several authors (Huh & Scriven 1971; and Dussan V. & Davis 1974) have shown that the application of the no-slip condition at a moving contact line gives rise to a non-integrable force singularity. The standard method of alleviating this problem is to allow for slipping of the fluid near the contact line (Dussan V. & Davis 1974; Huh & Mason 1977; Hocking 1977; and Davis 1983). In this paper a Navier slip condition of the form

$$u = \lambda(h)\, \boldsymbol{n}\cdot\boldsymbol{S}\cdot\boldsymbol{t} \tag{1.1}$$

is used where u is the tangential component of velocity along the wall, $\boldsymbol{n}$ and $\boldsymbol{t}$ are the unit normal and tangential vectors on the fluid solid interface, and taking μ to be the fluid viscosity, $\mu\boldsymbol{S}$ is the viscous stress tensor. The slip length $\lambda(h)$ is allowed to be a function of the drop height h, and we shall consider the three cases:

$$\lambda = \lambda_0, \quad \lambda = \frac{\lambda_1}{h}, \quad \lambda = \frac{\lambda_2}{h^2}, \tag{1.2a–c}$$

where λ_0, λ_1 and λ_2 are non-zero constants. Much of the work will use the slip model with $\lambda(h) = \lambda_1/h$.

Although we do not give an explicit derivation of our slip model (1.1), we note that recent analytical and numerical work does imply that such models are reasonable. For example, Jansons (1986) developed a model of a rough surface and was able to make theoretical predictions of the slip length. Also, recently Koplik, Banavar & Willemsen (1989), using a molecular-dynamics simulation of a low-Reynolds-number flow in a channel, have shown that the no-slip condition appears to break down near the contact line. We note that there has been a considerable amount of work which modifies the Navier–Stokes equations in the neighbourhood of the contact line by allowing for additional physics there (see e.g. the review article by de Gennes 1985). In terms of this work we can view the boundary condition (1.1) plus our slip velocity *vs.* contact angle relationship as effective boundary conditions which allow the use of the Navier–Stokes equations in the whole computational domain. For us the functional form of λ will be given by (1.2) but in principle it should be determined from the behaviour of the contact line with the additional physics. This could result, say, from a matched asymptotic analysis.

Here we shall use a lubrication model of the droplet. This model was developed by

Greenspan (1978) and has been used by several authors, see e.g. Greenspan & McCay (1981), Hocking (1981, 1983) and Rosenblat & Davis (1985). By assuming that the height of the droplet is much smaller than its radius Greenspan derived a first order in time, fourth order in space nonlinear partial differential equation for the motion of the free surface of an axisymmetric droplet. We should note that an alternative approach has been taken by Hocking & Rivers (1982) in which they avoid the lubrication approximation with its small contact angle requirement by considering droplets spreading at small capillary number with conditions of constant slip and constant contact angle.

In this paper we shall determine solutions of the lubrication equation for different slip models and contact angle versus velocity relationships. Also we wish to determine the spreading rate as a function of the physical parameters (Bond number, capillary number, etc.) in the problem. We note that there has been some previous work in this direction. For example Dussan V. (1976) did an analytical study of the steady motion of a droplet with different $\lambda(h)$ in the limit of small capillary and Reynolds number plus small deviation of the contact angle from its steady value. She found that the characteristic of the slip boundary condition which most affects the overall flow field is the magnitude of the slip length. Here we shall consider the initial-value problem for the motion of the drop. Although there have been some solutions in the literature (Hocking 1981, 1983) for the motion of droplets, the initial-value problem with various slip models and slip velocity–contact angle relationships has not been considered before. Since there is no one accepted slip model, it is important to determine how different models affect the droplet motion. Also, since several slip velocity–contact angle relationships have been used in the literature, it is important to understand their effect on the droplet motion. Our aim is to address these points here. We should note that Hocking (1983), using the lubrication model, determined the motion of a droplet at small capillary number with a constant-slip model ($1.2a$) and using a fixed contact angle. The small-capillary-number assumption gives a quasi-steady motion and allowed him to solve the problem using a matched asymptotic analysis.

This paper will be primarily concerned with solving the lubrication model numerically. This will be done by using a pseudo-spectral method. We shall use a Chebychev collocation method which will give very accurate information near the contact line. Much of the previous numerical work on this model has involved expansions in terms of powers of a radial variable measured from the centre of the drop (Greenspan & McCay 1981; Rosenblat & Davis 1985). For small capillary numbers such expansions can be expected to be good since the result at leading order in capillary number is a quadratic in terms of the radial variable. Numerical results at larger values of the capillary number and for very small slip lengths using these techniques are questionable because of the lack of resolution near the contact line. Another approach is due to Hocking (1981) who used a finite-difference method along with a clever spatial stretching near the contact line to study the motion of a two-dimensional drop. Few results were presented and only one model of the contact line was studied.

In order to understand the initial-value problem in detail, a short-time linearization about the initial conditions will be done. This analysis will be applied to different models for the slip and contact-line behaviour to examine their effects. We shall consider combinations of the two slip conditions, $\lambda = \lambda_0$ constant and $\lambda(h) = \lambda_1 h^{-1}$, with two slip velocity–contact angle relations, linear and $\Theta = \Theta_s$. One of these cases, $\Theta = \Theta_s$ and $\lambda = \lambda_0$, has been previously studied by Hocking (1981).

In the next section the problem formulation, slip condition, and velocity–angle relations used will be discussed. The third-section is concerned with the small-time linearizations. In §4 we shall present numerical solutions of the lubrication model and determine the effect of varying the physical parameters on the rate of spreading. The parameters considered are slip length, capillary number, drop volume, Bond number, and initial contact angle. Also, additional comparisons of the spreading rates are made for a linear, piecewise quadratic and cubic velocity–angle relations as well as comparisons for singular and non-singular slip models.

2. Problem formulation

Consider an axisymmetric drop of an incompressible viscous liquid on a flat surface. Let r be the radial variable measured from the centre of the drop, z the vertical variable measured from the solid surface, $h(r,t)$ the surface of the drop, and Θ the (contact) angle that the edge of the drop makes with the solid surface (see figure 1). Denoting the radial and vertical components of velocity as u and w respectively, the equations of motion are: conservation of mass

$$\frac{1}{r}\frac{\partial}{\partial r}(ru)+\frac{\partial}{\partial z}w=0; \tag{2.1}$$

conservation of momentum

$$\rho\left(\frac{\partial u}{\partial t}+u\frac{\partial u}{\partial r}+w\frac{\partial u}{\partial z}\right)=\mu\left(\nabla^2 u-\frac{u}{r^2}\right)-\frac{\partial p}{\partial r} \tag{2.2}$$

and

$$\rho\left(\frac{\partial w}{\partial t}+u\frac{\partial w}{\partial r}+w\frac{\partial w}{\partial z}\right)=\mu\nabla^2 w-\frac{\partial p}{\partial z}-\rho g. \tag{2.3}$$

Here p is the pressure, ρ the fluid density, and g the acceleration due to gravity.

Along the solid surface $z=0$ the boundary conditions are

$$w=0, \tag{2.4}$$

and the Navier slip condition (1.1)

$$u-\lambda(h)\left[\frac{\partial u}{\partial z}+\frac{\partial w}{\partial r}\right]=0. \tag{2.5}$$

The boundary conditions along the drop's surface $z=h(r,t)$ are the kinematic condition

$$\frac{\partial h}{\partial t}+u\frac{\partial h}{\partial r}-w=0, \tag{2.6}$$

the continuity of tangential stress

$$\frac{\partial h}{\partial r}\left(\frac{\partial u}{\partial r}-\frac{\partial w}{\partial z}\right)+\frac{1}{2}\left[\left(\frac{\partial h}{\partial r}\right)^2-1\right]\left(\frac{\partial w}{\partial r}+\frac{\partial u}{\partial z}\right)=0, \tag{2.7}$$

and the jump in normal stress

$$p=p_{\mathrm{A}}-\sigma\frac{1}{r}\frac{\partial}{\partial r}\left\{r\frac{\partial h}{\partial r}\left[1+\left(\frac{\partial h}{\partial r}\right)^2\right]^{-\frac{1}{2}}\right\}+2\mu\left[1+\left(\frac{\partial h}{\partial r}\right)^2\right]^{-1}\left[\left(\frac{\partial h}{\partial r}\right)^2\frac{\partial u}{\partial r}-\frac{\partial h}{\partial r}\left(\frac{\partial u}{\partial z}+\frac{\partial w}{\partial r}\right)+\frac{\partial w}{\partial z}\right]. \tag{2.8}$$

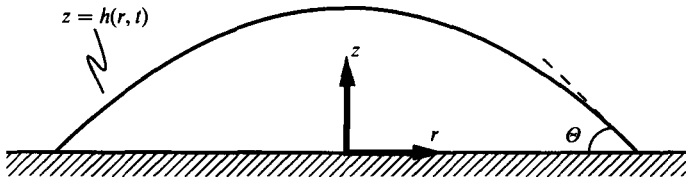

FIGURE 1. Drop profile with contact angle Θ.

Here σ is the surface tension and p_A is the ambient pressure above the droplet.

Boundary conditions are still needed at the contact line. The relation between the slip velocity U_S and the contact angle Θ is formally written as

$$U_S = f(\Theta). \tag{2.9a}$$

Since the slip velocity can be expressed in terms of the drop radius $R(t)$ as

$$U_S = \frac{dR}{dt} \tag{2.9b}$$

we can combine (2.9*a*, *b*) to give

$$\frac{dR}{dt} = f(\Theta). \tag{2.10}$$

We shall use the linear, piecewise quadratic and cubic relations

$$\frac{dR}{dt} = \kappa_1(\Theta - \Theta_S), \tag{2.11a}$$

$$\frac{dR}{dt} = \begin{cases} \kappa_2(\Theta - \Theta_S)^2, & \Theta \geqslant \Theta_S \\ -\kappa_2(\Theta - \Theta_S)^2, & \Theta < \Theta_S, \end{cases} \tag{2.11b}$$

$$\frac{dR}{dt} = \kappa_3(\Theta - \Theta_S)^3, \tag{2.11c}$$

where κ_1, κ_2 and κ_3 are constants, and θ_S is the unique static contact angle. Geometric considerations at the contact line yield two additional constraints on the drop surface $h(r, t)$. The first is that the surface of the drop must touch the solid surface there,

$$h[R(t), t] = 0. \tag{2.12}$$

Secondly, the contact angle is related to the slope of the drop by

$$\left.\frac{\partial h}{\partial r}\right|_{r=R(t)} = -\tan\Theta. \tag{2.13}$$

Finally, since the drop is assumed incompressible the volume V is a constant function of time. This is written as

$$V = 2\pi \int_0^{R(t)} rh(r, t)\, dr. \tag{2.14}$$

Given a set of initial conditions, then (2.1)–(2.8) with some form of (2.11), and (2.12)–(2.14) can be solved as functions in time. In general, however, this is very difficult as we are dealing with a moving-boundary problem and the Navier–Stokes equations. This problem is greatly simplified by using the lubrication approximation, which assumes that the ratio of the height to the radius of the droplet is small.

To analyse the above system, we introduce dimensionless coordinates consistent with the lubrication assumption. We shall assume that the drop height is small compared to its radius, and that the contact angle is correspondingly small. This implies that if Θ_0 is the characteristic contact angle then,

$$0 < \Theta_0 \ll 1. \tag{2.15}$$

Suppose we let R_C be a length characteristic of the drop radius, such as the initial drop radius or the equilibrium radius in those cases where Θ_s is non-zero. Then we can introduce the dimensionless variables

$$\left.\begin{array}{lll} t = \hat{t} R_C \mu/(\sigma \Theta_0^3), & r = \hat{r} R_C, & z = \hat{z} R_C \Theta_0, \\ u = \hat{u} \hat{\kappa} \Theta_0, & w = \hat{w} \hat{\kappa} \Theta_0^2, & \Theta = \hat{\Theta} \Theta_0, \\ p = \hat{p} \mu \hat{\kappa}/(R_C \Theta_0) + p_A, & R = \hat{R} R_C, & h = \hat{h} R_C \Theta_0, \\ V = \hat{V} 2\pi R_C^3 \Theta_0, & f = \hat{f} \hat{\kappa} \Theta_0. & \end{array}\right\} \tag{2.16a}$$

In addition, for each of the slip-velocity relationships in (2.11) we define $\hat{\kappa}$ as

$$\kappa_1 = \hat{\kappa}, \quad \kappa_2 = \hat{\kappa}/\Theta_0, \quad \kappa_3 = \hat{\kappa}/\Theta_0^2. \tag{2.16b}$$

Also for each of the models (1.2) of the slip coefficients $\lambda(h)$ we define the dimensionless slip parameter $\hat{\lambda}_i, i = 1, 2, 3$, as

$$\lambda_0 = \hat{\lambda}_0 (R_C \Theta_0), \quad \lambda_1 = \hat{\lambda}_1 (R_C \Theta_0)^2, \quad \lambda_2 = \hat{\lambda}_2 (R_C \Theta_0)^3. \tag{2.16c}$$

In the above scalings, we have kept velocities and lengths in the vertical direction much smaller than those in the radial, in keeping with the lubrication limit. We note that the constant $\hat{\kappa}$ is used to define the dimensionless velocities in (2.16*a*). This follows from the simple linear model (2.11*a*) where we see that $\mathrm{d}f/\mathrm{d}\Theta = \hat{\kappa}$. The definition of $\hat{\kappa}$ is modified for the quadratic (2.11*b*) and cubic (2.11*c*) case. For the constant-contact-angle case of $\Theta = \Theta_s$ we shall define the unit of velocity $\hat{\kappa}\Theta_0$ in terms of the characteristic length R_C and the characteristic time $R_C \mu/\sigma\Theta_0^3$. With these scalings, we also introduce the non-dimensional groupings of capillary number

$$Ca = \mu \hat{\kappa}/(\sigma \Theta_0^2), \tag{2.17}$$

Bond number

$$B = \rho g R_C^2/\sigma, \tag{2.18}$$

and Reynolds number

$$Re = \rho R_C \hat{\kappa}/\mu, \tag{2.19}$$

where all of these parameters are taken to be order 1.

Using (2.16)–(2.19) in the system (2.1)–(2.8), and (2.11)–(2.14) we obtain dimensionless equations for the fluid motion. This completed, we then drop the caret over the non-dimensional variables. Following the analysis of Greenspan (1978), we keep the leading-order terms in θ_0 and integrate the equations to get a partial differential equation for the drop surface $h(r,t)$ coupled with one for the drop radius $R(t)$. The resultant equation for $h(r,t)$ is

$$\frac{\partial h}{\partial t} = \frac{1}{r}\frac{\partial}{\partial r}\left(W \frac{\partial q}{\partial r}\right), \quad 0 < r < R(t) \tag{2.20}$$

where

$$\frac{\partial q}{\partial r} = \frac{\partial}{\partial r}\left[B h - \frac{1}{r}\frac{\partial}{\partial r}\left(r \frac{\partial h}{\partial r}\right)\right] \tag{2.21}$$

and

$$W = r[\tfrac{1}{3}h^3 + \lambda(h)\, h^2]. \tag{2.22}$$

The general velocity–angle relation (2.11) using (2.13) becomes

$$\frac{\mathrm{d}R}{\mathrm{d}t} = Caf\left(-\left.\frac{\partial h}{\partial r}\right|_{r=R}\right). \tag{2.23}$$

For boundary conditions, first consider the origin $r = 0$. Symmetry and smoothness at the centre of the droplet imply that

$$\left.\frac{\partial h}{\partial r}\right|_{r=0} = 0, \tag{2.24}$$

and

$$\left.\frac{\partial^3 h}{\partial r^3}\right|_{r=0} = 0. \tag{2.25}$$

At the contact line, the geometric condition (2.12) carries over directly. As for the volume constraint (2.14), its non-dimensional form is

$$V = \int_0^R rh(r,t)\,\mathrm{d}r. \tag{2.26}$$

Equations (2.12), (2.20)–(2.26) determine the motion of the droplet in the lubrication limit.

We note that (2.20) has four spatial derivatives so four boundary conditions are expected for a well-posed problem but only three (2.12), (2.24) and (2.25) are given. (The condition (2.23) determines the moving boundary.) For our problem three conditions are sufficient. One might expect that the volume constraint (2.26) gives an additional (global) condition, but this is not true. To demonstrate this, take a time derivative of (2.26), and use (2.12) to show that

$$\frac{\mathrm{d}V}{\mathrm{d}t} = \int_0^R r\frac{\partial h}{\partial t}\mathrm{d}r = 0. \tag{2.27}$$

Then using (2.20) to substitute for $\partial h/\partial t$, we can integrate once to get

$$W\frac{\partial q}{\partial r}\Bigg|_{r=0}^{r=R} = 0. \tag{2.28}$$

The product $W(\partial q/\partial r)$ is zero at $r = 0$, leaving only the end $r = R$ to be considered. For $\lambda(h) = \lambda_0$ and $\lambda(h) = \lambda_1 h^{-1}$, W is zero at the contact line, and we find that (2.20) is volume preserving. Therefore since W, the coefficient of the highest-order derivative, is zero at the contact line, (2.20) is singular there. So although we do not have an explicit proof, we expect, as with other differential equations where the coefficient of the highest derivative is zero at a boundary, to need one less boundary condition to determine a bounded solution of our problem. In other words we shall assume that (2.12) and (2.22)–(2.25) give a well-posed initial-value problem for $h(r,t)$ and $R(t)$. Because of (2.27) and (2.28) the volume constraint (2.26) can be used as a check on the accuracy of numerical method (see Haley 1990). For the $\lambda(h) = \lambda_2 h^{-2}$ case, W is not zero at $r = R$ and we need to force $\partial q/\partial r$ to be zero there. This is the required fourth boundary condition for the non-singular equation.

Before continuing we should note that the system (2.12) and (2.20)–(2.25) admits a steady-state solution, h_s, of the form (note $f(\Theta_s) = 0$)

$$h_s(r,\Theta_s,R_s) = \begin{cases} \frac{1}{2}\Theta_s R_s\left[1-\left(\frac{r}{R_s}\right)^2\right] & \text{if } B = 0 \\ \dfrac{\Theta_s}{B^{\frac{1}{2}}I_1(B^{\frac{1}{2}}R_s)}[I_0(B^{\frac{1}{2}}R_s)-I_0(B^{\frac{1}{2}}r)] & \text{if } B \neq 0. \end{cases} \tag{2.29}$$

Here we have that the steady profile is defined for $0 \leqslant r \leqslant R_s$ and $I_0(x)$ and $I_1(x)$ are the modified Bessel functions of order zero and one, respectively. By picking the parameters Θ_s, R_s and B we have uniquely determined the volume of h_s. We note that this solution will work for all of the choices of the slip velocity versus contact angle relation as long as Θ_s is a static contact angle.

3. Small-time analysis

We wish to consider the initial-value problem for the motion of a droplet. As initial data we shall assume that the shape is of the form of the steady-state shape (2.29) but the initial contact angle, Θ_0, will differ from the static contact angle Θ_s. This implies that the motion of the droplet is initially driven only by the local changes near the contact line, as the only equation not satisfied will be (2.23). Therefore the initial motion of the fluid in the neighbourhood of the contact line must be completely understood if we expect to obtain accurate numerical computations of the droplet motion.

Here we shall study this initial-value problem by using the method of matched asymptotic expansions (see, e.g. Van Dyke 1975). We shall consider four cases:

$$\text{(i)} \quad \lambda(h) = \frac{\lambda_1}{h} \quad \text{and} \quad f(\Theta) = \Theta - \Theta_s, \tag{3.1}$$

$$\text{(ii)} \quad \lambda(h) = \frac{\lambda_1}{h} \quad \text{and} \quad \Theta = \Theta_s, \tag{3.2}$$

$$\text{(iii)} \quad \lambda(h) = \lambda_0 \quad \text{and} \quad f(\Theta) = \Theta - \Theta_s, \tag{3.3}$$

$$\text{(iv)} \quad \lambda(h) = \lambda_0 \quad \text{and} \quad \Theta = \Theta_s, \tag{3.4}$$

with λ_0 and λ_1 given constants. Cases (i) and (ii) have a singular slip coefficient at the contact line, while the slip coefficient in cases (iii) and (iv) is a constant. Cases (i) and (iii) assume a linear relationship between the slip velocity, given by $\mathrm{d}R/\mathrm{d}t$ in (2.23), and the contact angle. On the other hand cases (ii) and (iv) assume that the contact angle is fixed for all positive time. This implies that the boundary condition (2.23) no longer applies for cases (ii) and (iv) and is replaced by the condition $\Theta = \Theta_s$. These four cases were chosen for our analysis because they have been used by several authors in studying contact-line motion. Here we would like to explicitly show how the four slip conditions influence the initial contact-line motion. Other slip conditions can be studied by a similar analysis. Hocking (1981) has already investigated the initial-value problem associated with case (iv). Parts of our analysis will parallel his.

With the system (2.20)–(2.25) and (2.12), choose the volume and initial conditions as

$$h(r, 0) = h_0(r), \tag{3.5}$$

$$R(0) = 1, \tag{3.6}$$

$$V = \int_0^1 r h_0(r)\, \mathrm{d}r, \tag{3.7}$$

where

$$h_0(r) = \begin{cases} \frac{1}{2}\Theta_0(1-r^2) & \text{if} \quad B = 0, \\ \dfrac{\Theta_0}{B^{\frac{1}{2}} I_1(B^{\frac{1}{2}})}[I_0(B^{\frac{1}{2}}) - I_0(B^{\frac{1}{2}} r)] & \text{if} \quad B \neq 0, \end{cases} \tag{3.8}$$

and Θ_0 is the initial contact angle. Notice that common to both these choices of $h_0(r)$ are the conditions $h_0(1) = 0$, and $(\partial h_0/\partial r)|_{r=1} = -\Theta_0$. Also we shall assume that the initial contact angle is close to the static contact angle (we will be specific about this shortly).

In order to study the initial motion of the contact line we need only consider the linearized problems about the initial conditions. If we define the deviations of height, radius and contact angle from the steady state as

$$\left.\begin{aligned} h(r,t) &= h_0(r)+h^*(r,t),\\ R(t) &= 1+R^*(t),\\ \Theta_s-\Theta_0 &= \psi, \end{aligned}\right\} \tag{3.9}$$

we find that the resulting linearized problem for case (i) is

$$\frac{\partial h^*}{\partial t} = \frac{1}{r}\frac{\partial}{\partial r}\left\{W_0\frac{\partial q^*}{\partial r}\right\}, \quad 0 < r < 1, \tag{3.10}$$

with

$$\frac{\partial q^*}{\partial r} = B\frac{\partial h^*}{\partial r} - \frac{\partial}{\partial r}\left\{\frac{1}{r}\frac{\partial}{\partial r}\left(r\frac{\partial h^*}{\partial r}\right)\right\} \tag{3.11}$$

and

$$W_0 = r[\tfrac{1}{3}h_0^3+\lambda_1 h_0]. \tag{3.12}$$

At $r = 1$ we have

$$\frac{\mathrm{d}R^*}{\mathrm{d}t} = -Ca\left\{\psi+\frac{\partial h^*}{\partial r}+R^*\frac{\partial^2 h_0}{\partial r^2}\right\} \tag{3.13}$$

and

$$h^*(1,t) = \Theta_0 R^*, \tag{3.14}$$

while at $r = 0$ we get the boundary conditions

$$\frac{\partial h^*}{\partial r} = \frac{\partial^3 h^*}{\partial r^3} = 0. \tag{3.15}$$

The volume integral (2.26) reduces to

$$\int_0^1 rh^*\,\mathrm{d}r = 0 \tag{3.16}$$

and as initial conditions we have

$$h^*(r,0) = R^*(0) = 0. \tag{3.17}$$

The system (3.10)–(3.17) will be solved by the method of matched asymptotics. The inner region will be in the neighbourhood of the contact line, while the outer region will be away from it.

Since (3.10)–(3.17) can be expected to hold only for short times, introduce the time stretching

$$t = \epsilon\tau \tag{3.18}$$

with ϵ a small parameter, $0 < \epsilon \ll 1$. We now look for the outer solution, away from the contact line, in terms of a regular perturbation expansion in ϵ. We see immediately that at leading order in ϵ, the perturbation to the height h^* is zero in the outer region. In other words, the initial motion of the drop is confined to the inner region.

Now consider the inner region. Here the drop height is small and distances will be

measured local to the position of the contact line $r = R(t)$. Therefore, introduce the scalings near the contact line of

$$s = \frac{1-r}{\epsilon^{\frac{1}{3}}}, \tag{3.19}$$

$$h^*(r,\tau) = \epsilon H(s,\tau), \tag{3.20}$$

and

$$R^*(\tau) = \epsilon \bar{R}(\tau) \tag{3.21}$$

into (3.10)–(3.17) and group in powers of ϵ. Keeping the terms of leading order in ϵ, we find

$$\frac{\partial H}{\partial \tau} = -\frac{\partial}{\partial s}\left(\lambda_1 \Theta_0 s \frac{\partial^3 H}{\partial s^3}\right), \tag{3.22}$$

$$\frac{\mathrm{d}\bar{R}}{\mathrm{d}\tau} = -Ca\,\psi, \tag{3.23}$$

$$H(0,\tau) = \Theta_0 \bar{R}(\tau), \tag{3.24}$$

$$\int_0^\infty H(s,\tau)\,\mathrm{d}s = 0, \tag{3.25}$$

$$H(s,0) = 0, \tag{3.26}$$

$$\bar{R}(0) = 0, \tag{3.27}$$

and the matching condition

$$\lim_{s\to\infty} H(s,\tau) = 0. \tag{3.28}$$

Equation (3.25) and the matching condition (3.28) arise because the outer solution is zero at this order. We note that this system holds for the Bond number B both zero and non-zero. This occurs because $h_0(r)$ looks linear to this order, and both cases look like the same line.

From (3.23) and (3.27) we see that the equation for $\bar{R}(\tau)$ decouples from those for $H(s,\tau)$. We find that the solution for $\bar{R}(\tau)$ is given by

$$\bar{R}(\tau) = -Ca\,\psi\tau. \tag{3.29}$$

Using this in (3.24) the boundary condition for H becomes

$$H(0,\tau) = -Ca\,\psi\Theta_0\tau. \tag{3.30}$$

We can now look for a similarity solution to the system (3.22), (3.25), (3.26), (3.28), and (3.30). Define the similarity variables

$$x = \frac{s}{(\lambda_1 \Theta_0 \tau)^{\frac{1}{3}}}, \tag{3.31}$$

$$H(s,\tau) = \psi\, Ca\, \Theta_0 \tau F_1(x), \tag{3.32}$$

and substitute them into the system. We get in the inner region the similarity problem

$$\frac{\mathrm{d}}{\mathrm{d}x}(xF_1'''(x)) - \tfrac{1}{3}xF_1'(x) + F_1(x) = 0, \tag{3.33}$$

with

$$F_1(0) = -1, \tag{3.34}$$

$$\lim_{x\to\infty} F_1(x) = 0, \tag{3.35}$$

and
$$\int_0^\infty F_1(x)\,\mathrm{d}x = 0. \tag{3.36}$$

Equation (3.33) is a fourth-order ordinary differential equation for $F_1(x)$. It must satisfy the two boundary conditions (3.34) and (3.35) plus the integral constraint (3.36). Again we appear to be missing one condition for this fourth-order equation but, as noted earlier, the equation is singular at $x = 0$ so we need only the above conditions to determine bounded solutions.

We can solve (3.33) by noting that it can be converted to a first-order equation by using a Laplace transform. This then, at least formally, is solved fairly straightforwardly. Unfortunately, the resulting solution is very difficult to use. Therefore we shall solve the system numerically. Two additional conditions at $x = 0$ can be determined by looking at the exact solution near $x = 0$ to find

$$F_1'''(0) = 1, \tag{3.37}$$

and
$$F_1'(0) = 3^{\frac{2}{3}}\left[2\int_0^1 \frac{y}{(1-y^3)^{\frac{1}{3}}}\mathrm{d}y\right]^{-1}. \tag{3.38}$$

This system is then solved numerically by using a variable-step-size finite-difference method (IMSL routine DBVPFD).

The other three cases can be solved in a similar manner. The difference will be the local scalings in the inner region and the similarity variables. Each case will have a slightly different differential equation for the surface. For case (ii) we set

$$x = \frac{1-r}{(\lambda_1 \Theta_0 \epsilon\tau)^{\frac{1}{3}}}, \tag{3.39}$$

$$h^*(r,\tau) = \psi(\lambda_1 \Theta_0 \epsilon\tau)^{\frac{1}{3}} F_2(x). \tag{3.40}$$

The equation for F_2 is

$$\frac{\mathrm{d}}{\mathrm{d}x}[xF_2'''] - \frac{x}{3}F_2' + \tfrac{1}{3}F_2 = 0, \tag{3.41}$$

$$F_2'(0) = 1, \tag{3.42}$$

$$\lim_{x\to\infty} F_2(x) = 0, \tag{3.43}$$

$$\int_0^\infty F_2(x)\,\mathrm{d}x = 0. \tag{3.44}$$

For case (iii) we have $\lambda(h) = \lambda_0$, and the linear velocity–angle relation

$$x = \frac{1-r}{\Theta_0(\lambda_0 \epsilon\tau)^{\frac{1}{2}}}, \tag{3.45}$$

$$h^*(r,\tau) = Ca\,\Theta_0 \psi \epsilon\tau F_3(x). \tag{3.46}$$

The equation for F_3 is now

$$\frac{\mathrm{d}}{\mathrm{d}x}[x^2F_3'''] - \tfrac{1}{2}xF_3' + F_3 = 0, \tag{3.47}$$

$$F_3(0) = -1, \tag{3.48}$$

$$\lim_{x\to\infty} F_3(x) = 0, \tag{3.49}$$

$$\int_0^\infty F_3(x)\,\mathrm{d}x = 0. \tag{3.50}$$

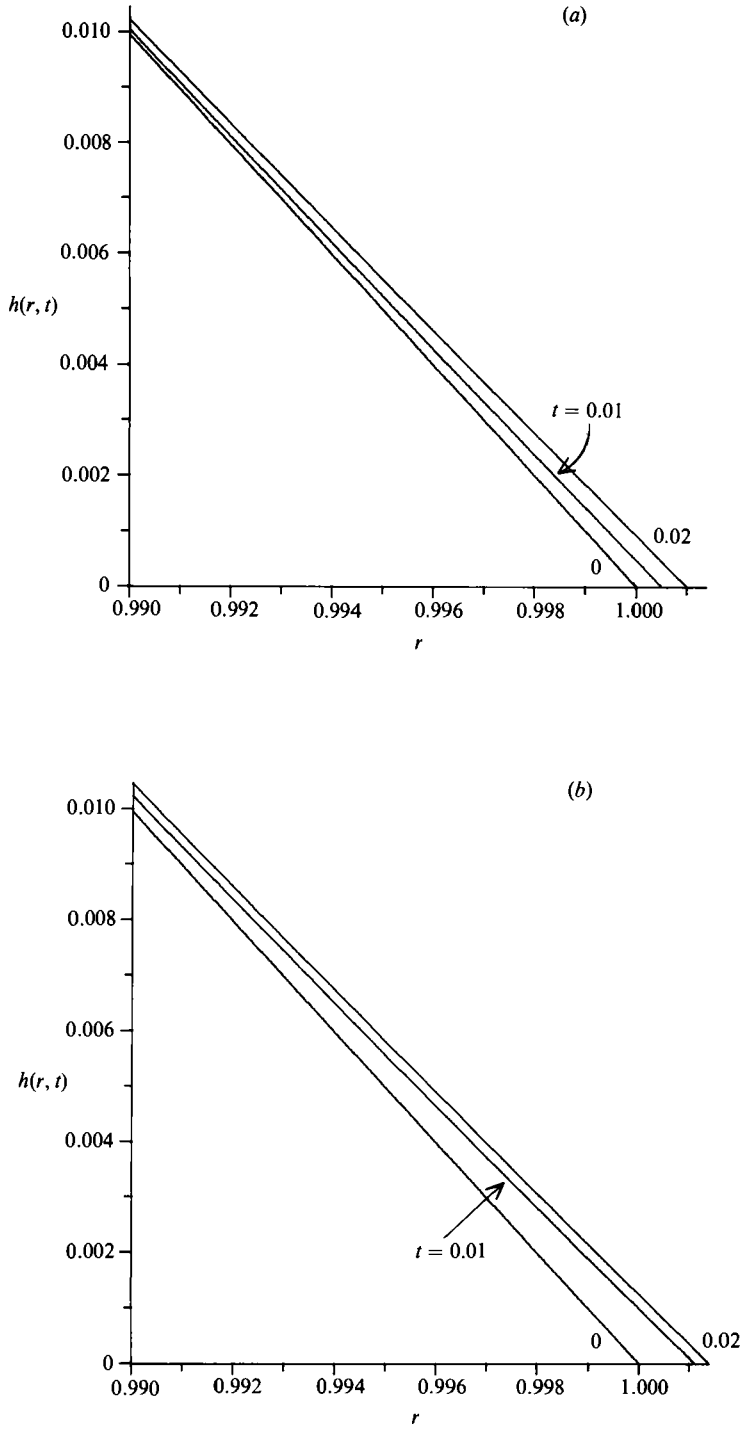

FIGURE 2(a, b). For caption see facing page.

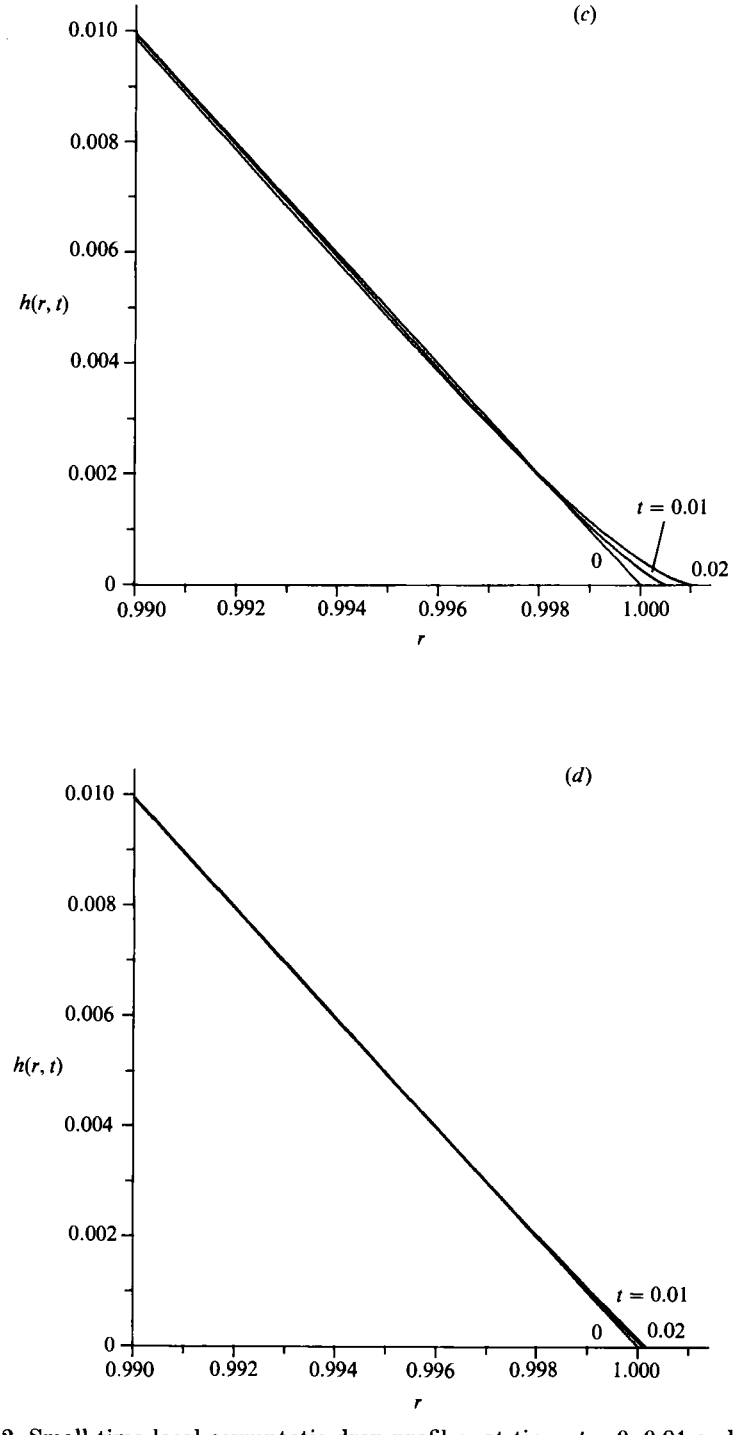

FIGURE 2. Small-time local asymptotic drop profiles, at times $t = 0$, 0.01 and 0.02. (*a*) case (i); (*b*) case (ii); (*c*) case (iii); (*d*) case (iv).

U_s *vs.* Θ relation and slip condition / Quantities compared	Case (i) $\frac{\lambda_1}{h}$, linear	Case (ii) $\frac{\lambda_1}{h}$, fixed angle	Case (iii) λ_0, linear	Case (iv) λ_0, fixed angle
$R(t)-1=$	$(\Theta_0-\Theta_s)Ca\,t$	$\dfrac{3^{\frac{1}{3}}(\Theta_0-\Theta_s)}{2\displaystyle\int_0^1(1-u^3)^{\frac{1}{3}}\,du}\left(\dfrac{\lambda_1 t}{\Theta_0^2}\right)^{\frac{1}{3}}$ $\approx 0.81638(\Theta_0-\Theta_s)\left(\dfrac{\lambda_1 t}{\Theta_0^2}\right)^{\frac{1}{3}}$	$(\Theta_0-\Theta_s)Ca\,t$	$\dfrac{4}{\pi^{\frac{3}{2}}}(\Theta_0-\Theta_s)(\lambda_0 t)^{\frac{1}{2}}$ $\approx 0.71835(\Theta_0-\Theta_s)(\lambda_0 t)^{\frac{1}{2}}$
As r moves away from contact line, $\lvert h(r,t)-h_0(r)\rvert \propto$	$x^{-\frac{4}{3}}\exp\left[\dfrac{-x}{2(3)^{\frac{1}{3}}}\right]$	$x^{-\frac{2}{3}}\exp\left[\dfrac{-x}{2(3)^{\frac{1}{3}}}\right]$	$x^{-\frac{2}{3}}\exp\left[\dfrac{-3}{2^{\frac{7}{3}}}x^{\frac{2}{3}}\right]$	$x^{-\frac{1}{3}}\exp\left[\dfrac{-3}{2^{\frac{5}{3}}}x^{\frac{2}{3}}\right]$
(equation for x)	(3.31)	(3.39)	(3.45)	(3.51)
Singular behaviour near contact line, $r=R(t)$, for $t>0$	h and all its r-derivatives are bounded	h and all its r-derivatives are bounded	$h_{rr}\sim\dfrac{Ca(\Theta_s-\Theta_0)}{R^2(t)\lambda_0\Theta_0}$ $\times\ln\left(\dfrac{1-r/R(t)}{\Theta_0(\lambda_0 t)^{\frac{1}{2}}}\right)$	$h_{rr}\sim\dfrac{2(\Theta_s-\Theta_0)}{\pi^{\frac{3}{2}}R^2(t)\,\Theta_0(\lambda_0 t)^{\frac{1}{2}}}$ $\times\ln\left(\dfrac{1-r/R(t)}{\Theta_0(\lambda_0 t)^{\frac{1}{2}}}\right)$
Jump in derivative from initial data at contact line	$\lim_{t\to 0^+} h_{rrr}[R(t),t]-h_{rrr}(1,0)$ $=\dfrac{Ca}{\lambda_1}(\Theta_0-\Theta_s)$	$h_r(1,0)=-\Theta_0$ but $h_r[R(t),t]=-\Theta_s$ for $t>0$	$h_{rr}(1,0)=h_0''(1)$ but $h_{rr}(r,t)$ is singular at the contact line for $t>0$	$h_r(1,0)=-\Theta_0$ but $h_r[R(t),t]=-\Theta_s$ for $t>0$

TABLE 1. Local behaviour near the contact line $r=R(t)$: the spreading, deviation from the initial conditions, lowest-order derivative singularity and lowest-order jump in time are contrasted for the four short-time analyses at leading order in ϵ

Finally for case (iv) we set $\lambda(h) = \lambda_0$, and fix the slip velocity–contact angle relation, so

$$x = \frac{1-r}{\Theta_0(\lambda_0 \epsilon \tau)^{\frac{1}{3}}}, \tag{3.51}$$

$$h^*(r,\tau) = \psi\Theta_0(\lambda_0 \epsilon\tau)^{\frac{1}{3}}F_4(x). \tag{3.52}$$

Here we find that

$$\frac{\mathrm{d}}{\mathrm{d}x}[x^2F_4'''] - \tfrac{1}{2}xF_4' + \tfrac{1}{2}F_4 = 0, \tag{3.53}$$

$$F_4'(0) = 1, \tag{3.54}$$

$$\lim_{x\to\infty} F_4(x) = 0. \tag{3.55}$$

In this last system, which was studied by Hocking (1981), the equation with its two boundary conditions imply conservation of volume.

We observe a rough qualitative agreement when we compare the composite solutions for $h(r,t)$ in figure 2. An initial lip of fluid flows out from the contact line, taking fluid from immediately above, and leaving the bulk of the drop undisturbed. As the motion progresses, more of the fluid above is drawn to the lip, until the entire drop feels the motion of the contact line. The singular slip length, $\lambda_1 h^{-1}$, cases, figure 2(*a*, *b*), involves more of the drop in the motion, while the non-singular cases, figure 2(*c*, *d*), keep the motion localized near the contact line. Although the profiles in figure 2(*a*, *b*), for the singular slip models, appear to show an increase in volume, this is an artifice of our using the same axes for all four cases. Were more of the drops in figure 2(*a*, *b*) shown, we would see profiles similar to figure 2(*c*, *d*). For the linear cases (i) and (iii) we find that $R(\tau)$ and H decouple and $R(\tau)$ is a linear function of τ depending only on the parameters Ca, Θ_0, and Θ_s. Consequently, the drop radius spreads in exactly the same manner initially regardless of the choice of $\lambda(h)$. For the constant-angle cases (ii) and (iv) we also find that $R(\tau)$ and H decouple but leave the drop radius a function of the similarity solution at the contact line. This makes the rate of spreading indirectly dependent upon the choice of $\lambda(h)$. In this case the singular choice spreads significantly faster.

Although an analytical solution for F_1, F_2, F_3 and F_4 is not obvious, we can determine the behaviour of F_i for large values of their similarity variable x using the WKB method. The result is in the far field of the inner region:

for case (i)

$$F_1(x) \sim x^{-\frac{4}{3}}\exp\left[-\frac{x}{2(3)^{\frac{1}{3}}}\right]\left\{A\cos\left(\frac{3^{\frac{1}{6}}}{2}x\right) + B\sin\left(\frac{3^{\frac{1}{6}}}{2}x\right)\right\}; \tag{3.56}$$

for case (ii)

$$F_2(x) \sim x^{-\frac{2}{3}}\exp\left[-\frac{x}{2(3)^{\frac{1}{3}}}\right]\left\{A\cos\left(\frac{3^{\frac{1}{6}}}{2}x\right) + B\sin\left(\frac{3^{\frac{1}{6}}}{2}x\right)\right\}; \tag{3.57}$$

for case (iii)

$$F_3(x) \sim x^{-\frac{2}{3}}\exp\left[-\frac{3}{2^{\frac{7}{3}}}x^{\frac{2}{3}}\right]\left\{A\cos\left(\frac{3^{\frac{3}{2}}}{2^{\frac{7}{3}}}x^{\frac{2}{3}}\right) + B\sin\left(\frac{3^{\frac{3}{2}}}{2^{\frac{7}{3}}}x^{\frac{2}{3}}\right)\right\}; \tag{3.58}$$

while for case (iv)

$$F_4(x) \sim x^{-\frac{1}{3}}\exp\left[-\frac{3}{2^{\frac{7}{3}}}x^{\frac{2}{3}}\right]\left\{A\cos\left(\frac{3^{\frac{3}{2}}}{2^{\frac{7}{3}}}x^{\frac{2}{3}}\right) + B\sin\left(\frac{3^{\frac{3}{2}}}{2^{\frac{7}{3}}}x^{\frac{2}{3}}\right)\right\}. \tag{3.59}$$

These results are summarized in table 1. In particular we note there the singular behaviour of h and its derivatives. The singular-slip-coefficient case has bounded

derivatives at the contact line but the constant-slip-coefficient cases will both have a logarithmic singularity at the contact line. Also we note that the fixed-contact-angle case will have a jump in its first derivative at time zero because the initial contact angle is not equal to the advancing contact angle. These results indicate that greater care will be needed in solving the initial-value problem for the fixed-angle cases, and that case (i) should have the fewest problems of the four.

4. Numerical method and results

Here we shall numerically solve the system of equations (2.12), (2.20)–(2.25) using a pseudo-spectral method (see e.g. Gottlieb & Orszag 1977 or Canuto *et al.* 1988). We begin by mapping our moving-boundary problem onto a fixed domain with the change of variables

$$t = \tau, \tag{4.1}$$

$$r = R(\tau)(x+1)/2, \tag{4.2}$$

$$h(r,t) = R(\tau)H(x,\tau). \tag{4.3}$$

The computational domain is now given by $\tau > 0$ and $-1 \leqslant x \leqslant 1$. This particular spatial domain is chosen for the Chebychev pseudo-spectral approximation of the spatial derivatives. To update in time we use a backward Euler method. Although only first order, it is very robust, being less sensitive to nonlinear instabilities than higher-order methods. This nonlinear system is solved by Newton's method. Details of this method as well as convergence checks can be found in Haley (1990).

We now present numerical solutions of the lubrication model of droplet motion. We shall begin by considering a linear contact angle–slip velocity relation (2.11*a*) and solving the system of equations with $\lambda(H) = \lambda_1/H$. Unless otherwise stated, we shall assume that the reference-case conditions are $B = 0$, $Ca = 0.1$, $\lambda_1 = 0.01$, $\Theta_s = 0$, $\Theta_0 = 1$, $R(0) = 1$ and we fix the volume $V = \frac{1}{8}$. The initial data are given by $h_s(r, \Theta_0, R(0))$ with $B = 0$, i.e. (2.29) with $B = 0$. In figure 3 we present several drop profiles for these conditions.

We note that if Θ_s were greater than zero but less than Θ_0 we would see the droplet asymptotically approach its equilibrium shape as time increases. Hence the case of $\Theta_s = 0$ is a reasonable problem to investigate since its behaviour is similar to that of all droplets which will try to coat a surface after it is initially deposited. If Θ_s were greater than Θ_0 the drop would contract and as time increased we would see the equilibrium shape asymptotically approached. As was observed by Greenspan & McCay (1981) it is possible in this case for the middle to decrease in height and then increase.

The first question we ask is how will the Bond number affect the spreading rate. In figure 4 we plot $R(t)$ *vs.* t for $B = 0$, 0.5, 1.0, 5.0 and 10.0. We find that increasing Bond number increases the spreading rate. Since B is proportional to g, the acceleration due to gravity, this is expected. We note that at $t = 50$ the difference between $B = 0$ and $B = 1$ is about 2% while the difference between $B = 1$ and $B = 10$ is about 14%. Here we should keep in mind that for $B \neq 0$ the initial data are not in equilibrium all along the surface of the drop and not just at the contact line.

Suppose we consider the effect of varying the drop volume on the spreading rate. Since our initial conditions are given by $h_s(r, \Theta_0, R(0))$ with $B = 0$, we find that the volume V, initial contact angle Θ_0 and initial radius $R(0)$ are related by

$$V = \tfrac{1}{8}\Theta_0 R^3(0). \tag{4.4}$$

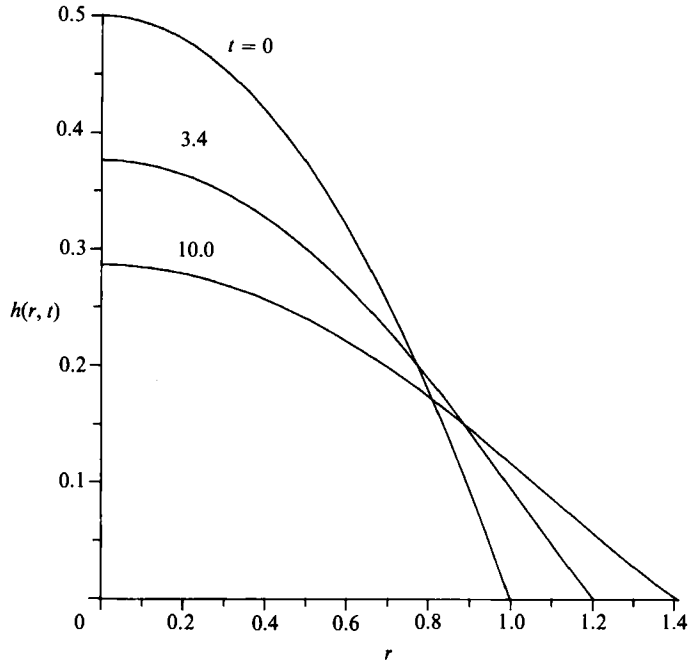

FIGURE 3. Drop profiles for the reference case at $t = 0$, 3.4 and 10.0.

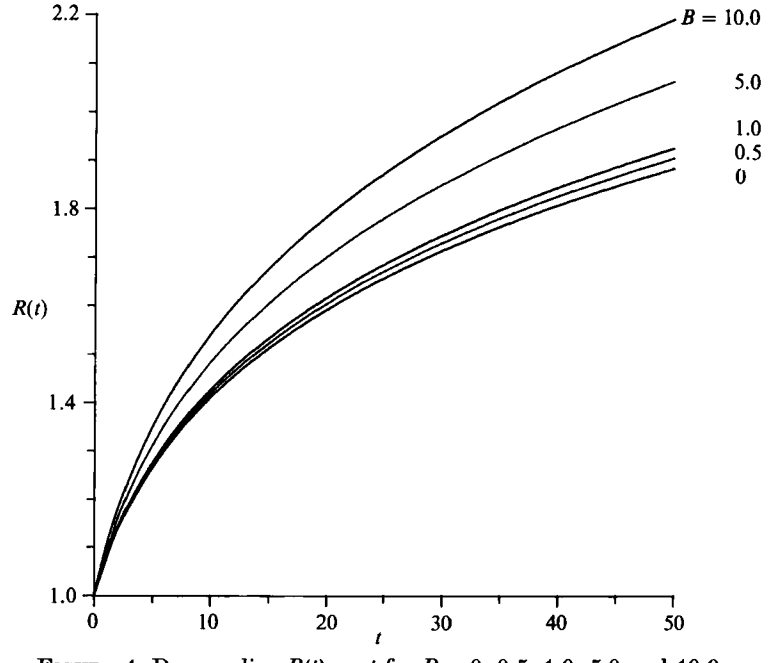

FIGURE 4. Drop radius $R(t)$ *vs.* t for $B = 0$, 0.5, 1.0, 5.0 and 10.0.

We first vary the volume by varying Θ_0. This is done in figure 5 where we consider the three cases of $\Theta_0 = 0.5$, 1.0 and 2.0. We find that the larger Θ_0 is, the faster the droplet spreads. Since a larger Θ_0 and fixed $R(0)$ implies a larger volume of the drop, we see that the spreading rate increases with volume. The latter observation is not

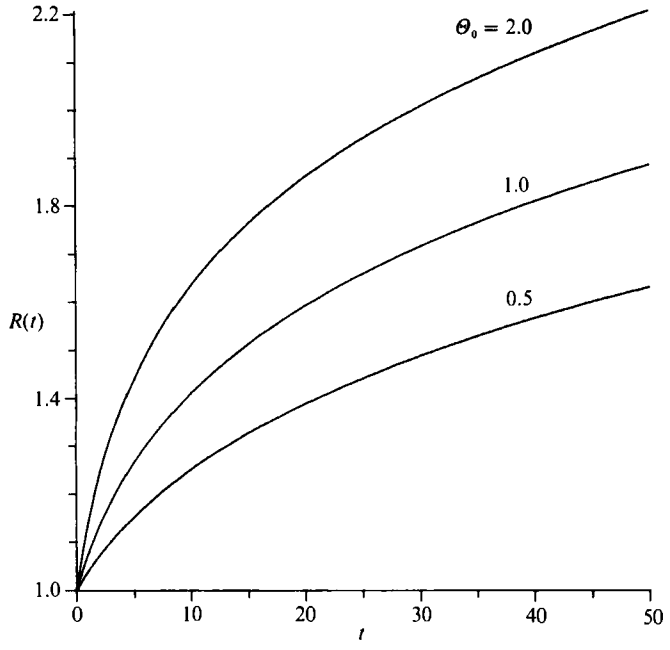

FIGURE 5. $R(t)$ *vs.* t for $\Theta_0 = 0.5$, 1.0 and 2.0 and for fixed initial radius $R(0) = 1$.

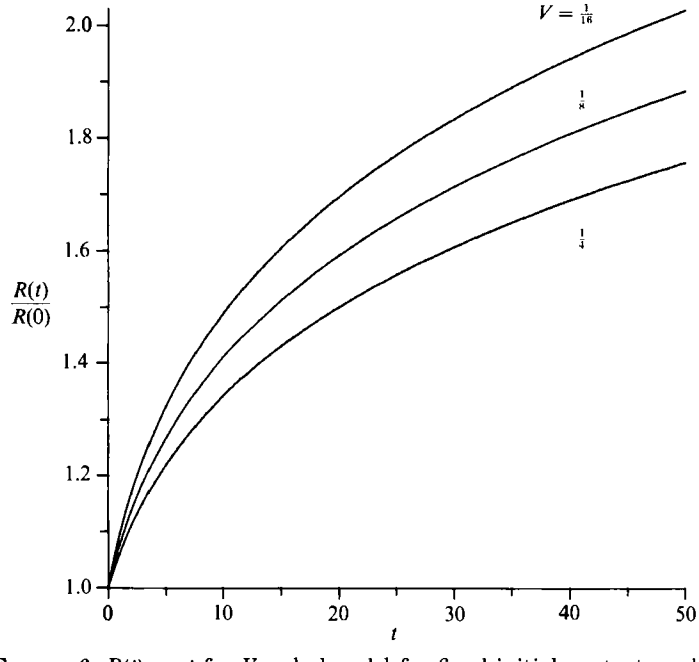

FIGURE 6. $R(t)$ *vs.* t for $V = \frac{1}{16}, \frac{1}{8}$ and $\frac{1}{4}$ for fixed initial contact angle $\Theta_0 = 1$.

in general true. In figure 6 we keep $\Theta_0 = 1$ fixed but considered the three cases of $V = \frac{1}{16}, \frac{1}{8}$ and $\frac{1}{4}$. From (4.4) we see that this implies that the initial radius must vary. So we plot the normalized radius $R(t)/R(0)$ versus t in figure 6. Here we see that the rate of increase of radius increases with decreasing volume, in contrast to the

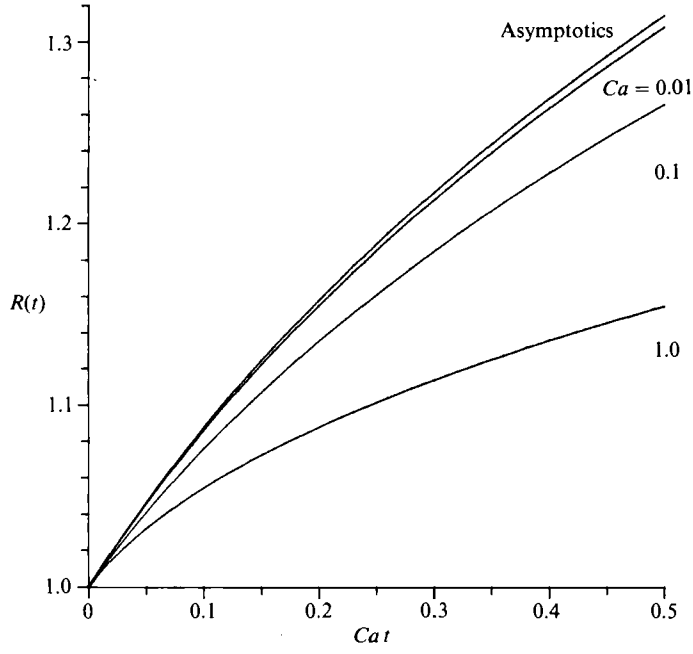

FIGURE 7. $R(t)$ *vs.* $Ca\,t$ for $Ca = 1.0$, 0.1 and 0.01 plus the small-Ca asymptotic limit (4.6).

previous case. These results imply that the spreading rate in this problem depends on two of the three parameters, $R(0)$, V and Θ_0. In other words, the initial values of all the parameters are needed to correctly interpret the results.

For small capillary number an asymptotic solution of (2.12), (2.20)–(2.25) can be found (see Greenspan 1978; Greenspan & McCay 1981). The result of the analysis for $B = 0$ is a first-order ordinary differential equation for the leading-order behaviour of $R(t)$:

$$\frac{dR}{dT} = -\Theta_s + \frac{8V}{R^3}, \tag{4.5}$$

where $T = t\,Ca$. For the special case of $\Theta_s = 0$ we can explicitly integrate (4.5) to find

$$R(t) = [32V\,Ca\,t + R^4(0)]^{\frac{1}{4}}. \tag{4.6}$$

In figure 7 we plot the drop radius versus the scaled time $T = Ca\,t$ for $Ca = 0.01$, 0.1 and 1.0. Also, we plot the asymptotic result (4.6). We see that the $Ca = 0.01$ case is very close to the asymptotic result even up to $t = 50$ with the difference less than 0.5%. For the $Ca = 0.1$ case, the asymptotic and numerical results differ by about 4% at $t = 5.0$ while at $t = 0.5$ the $Ca = 1$ numerical case has already differed from the asymptotic by 12%. So for $Ca < 0.1$ we can expect reasonable predictions from (4.5).

The two major modelling assumptions in this study are the form of the slip parameter $\lambda(H)$ and the slip velocity versus contact angle relationship. We now wish to study how these relationships affect the spreading rates. As noted before, Dussan V. (1976) has considered the limits of small capillary number and small $\Theta_0 - \Theta_s$ of a steady flow. Her conclusion was that the characteristic of the slip boundary condition that most affects the overall flow field is the magnitude of the slip length. For the initial-value problem studied here we shall not restrict ourselves to the assumptions of small capillary number and small $\Theta_0 - \Theta_s$ difference.

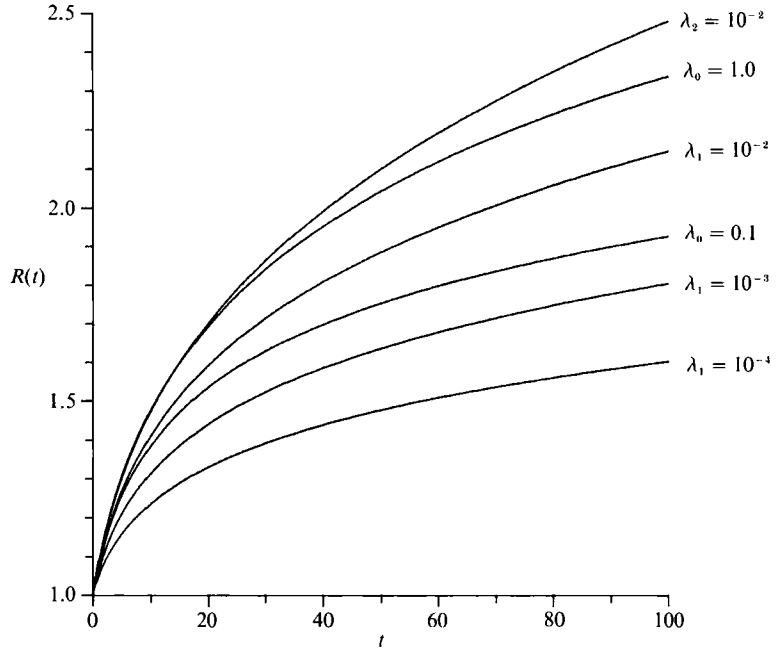

FIGURE 8. $R(t)$ *vs.* t for $\lambda_0 = 0.1$ and 1.0. Also for $\lambda_1 = 10^{-2}$, 10^{-3} and 10^{-4}, and for $\lambda_2 = 10^{-2}$.

In figure 8 we plot $R(t)$ *vs.* t for $\lambda_1 = 10^{-2}$, 10^{-3} and 10^{-4}. The other parameters are set to those of the basic-state case. We note that the spreading rate increases with λ_1. This result is consistent with the fact that the size of λ_1 can be viewed as a measure of the deviation of our slip model from the no-slip boundary condition, i.e. the larger λ_1 is then the more slip we find. We also show in figure 8 numerical results for a constant slip parameter, i.e. $\lambda(H) = \lambda_0$, case (iii) of §3, and set $\lambda_0 = 0.1$ and 1.0, as well as results for a quadratically singular slip parameter, $\lambda(H) = \lambda_2 H^{-2}$ with $\lambda_2 = 10^{-2}$. The qualitative behaviour of the spreading is similar in all three cases. In particular, the larger the slip coefficient, the larger the spreading rate. But there are some specific differences. For example in order to get approximately the same initial spreading rate the coefficient λ_0 in the non-singular case must be a lot larger than the λ_1 in the singular case. This is consistent with the observation that local to the contact line the singular slip coefficient will always be larger than any constant slip coefficient. Comparing the quadratically singular case to the singular case with $\lambda_1 = 0.01$ we again see that the case with the more singular slip function spreads faster. Further, as the drop spreads and thins, this effect is multiplied. This implies that we can expect that even if the initial spreading rate for the more singular case is slower than the less singular case, it will eventually overtake the less singular slip coefficient case (note that $\Theta_s = 0$ here). Although not shown in the graphs, we have also found that the less singular cases are gradually overtaken by the more singular cases for initial data where the more singular case initially spread slower than the less singular. In other words, after a sufficiently long time, a more singular case will always pass a less singular one.

The second major modelling assumption made was the contact angle–slip velocity relationship (2.11). We have assumed a linear relationship in all the results presented so far. In figure 9 we plot the radius $R(t)$ versus time t for the linear (2.11*a*), quadratic (2.11*b*) and cubic (2.11*c*) contact angle *vs.* slip velocity relationships. In

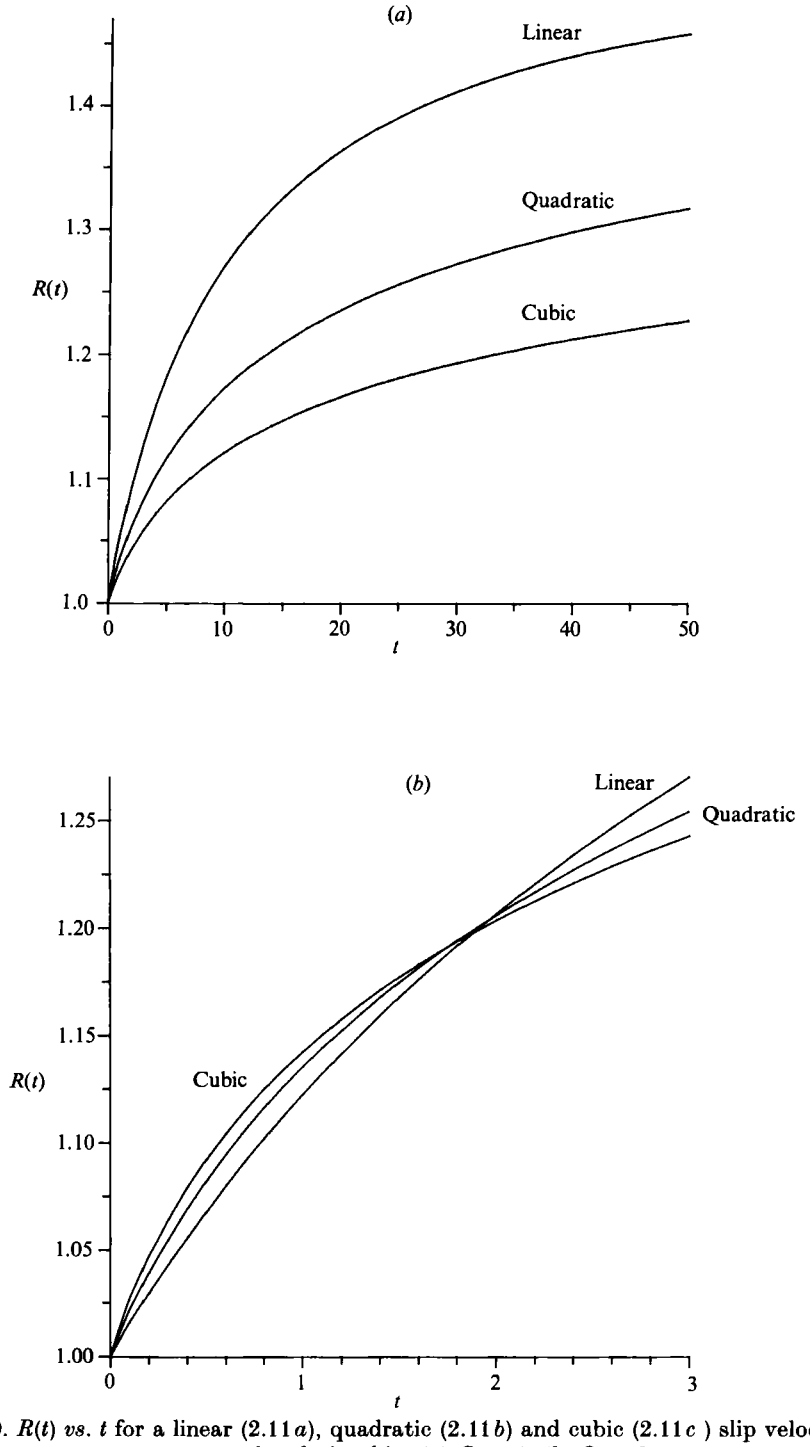

FIGURE 9. $R(t)$ *vs.* t for a linear (2.11*a*), quadratic (2.11*b*) and cubic (2.11*c*) slip velocity *vs.* contact-angle relationship. (*a*) $\Theta_0 = 1$, (*b*) $\Theta_0 = 2$.

figure 9(*a*) we set $\Theta_0 = 1$ and all of the other variables equal to the reference case. We find that the linear relation implies the fastest spreading, the quadratic the next and the cubic is the slowest. This is consistent with the fact that the droplet is spreading, so immediately the contact angle will drop below its initial angle $\Theta_0 = 1$. Therefore the right-hand side of (2.11*c*) will be smaller than the right-hand side of (2.11*b*) which will be smaller than the right-hand side of (2.11*a*). In figure 9(*b*) we set $\Theta_0 = 2.0$ (note the change in scales). Initially the cubic now spreads the fastest but eventually Θ will be less than one and the quadratic and linear cases will overtake it.

As with the linear case, a small-capillary-number limit can be considered for (2.11*b*) and (2.11*c*). The result is an equation similar to (4.5). For the quadratic case we find, at leading order in Ca with $B = 0$,

$$\frac{dR}{dT} = \left(-\Theta_s + \frac{8V}{R^3}\right)^2, \tag{4.7}$$

and for the cubic,

$$\frac{dR}{dT} = \left(-\Theta_s + \frac{8V}{R^3}\right)^3, \tag{4.8}$$

where $T = Ca\,t$ with the respective Ca for each case. For $\Theta_s = 0$ we can integrate to find that, at leading order in Ca,

$$R(t) = [7(8V)^2 Ca\,t + R^7(0)]^{\frac{1}{7}} \tag{4.9}$$

for the quadratic relation (2.11*b*), while

$$R(t) = [10(8V)^3 Ca\,t + R^{10}(0)]^{\frac{1}{10}} \tag{4.10}$$

for the cubic relation (2.11*c*). Here we see that for large times R grows like $t^{\frac{1}{7}}$ for the linear relationship (2.11*a*), like $t^{\frac{1}{7}}$ for the quadratic relationship (2.11*b*) and like $t^{\frac{1}{10}}$ for the cubic relationship (2.11*c*). We note that these spreading rates were obtained by de Gennes (1985) by a different argument.

Recently Chen (1988) did a series of experiments on the spreading of a liquid drop with a very small advancing static contact angle (less than 1°). For his experiments (silicone oil drop on a soda-lime glass plate) he found that the radius grew as $t^{\frac{1}{10}}$. He compared these predictions with a solution given by Starov (1983). Starov found this solution by looking for a similarity solution of (2.20) with $\lambda(h) = 0$. Starov's calculation assumes that the surface is wetted and he defines the contact line as the point of inflection in the profile. We have recovered this $t^{\frac{1}{10}}$ spreading by just assuming (2.11*c*) and allowing for a contact angle. We note that (2.11*c*) predicts that the contact angle decays as $t^{-\frac{1}{3}}$. This is also predicted by Starov (1983). We also note that our small-Ca results (4.5), (4.7) and (4.8) should also be approximately valid at large time and not just small values of Ca. This follows since, as the drop spreads, the profile should be approximately the static shape, a quadratic (2.29) for $B = 0$. This is exactly the result of the small-Ca analysis. Then using either (2.11*a*), (2.11*b*) or (2.11*c*) the equation for the radius follows, either (4.5), (4.7) or (4.8). We should also note that Hocking (1983) using the constant-slip and constant-contact-angle conditions predicts approximately the $t^{\frac{1}{10}}$ spreading rate by including lower-order terms in the small-capillary-number expansion.

In figure 10 we compare the small-time asymptotic result for the reference case (i.e. case (i) of §3) to the numerical solution of the reference case for $Ca = 0.001$, 0.01, 0.1 and 1.0. We plot the radius $R(t)$ versus $T = Ca\,t$. For fixed T we note that the numerical results approach the asymptotic as the capillary number decreases. In terms of the time t, this implies that the small-capillary-number runs will have better agreement with the asymptotic results for larger values of t.

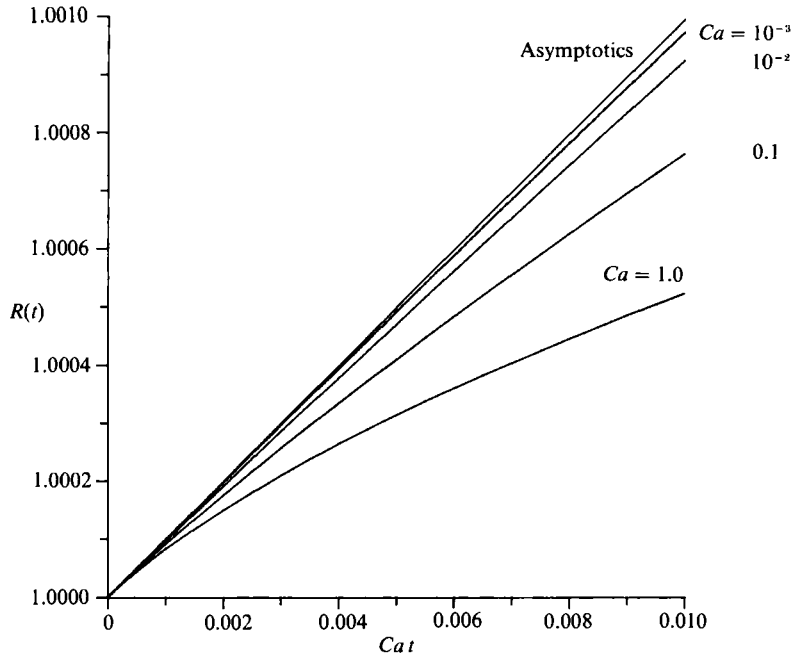

FIGURE 10. $R(t)$ *vs.* $Ca\,t$ for $Ca = 0.001$, 0.01, 0.1, 1.0 and the small-time asymptotic result of case (i).

Slip condition $\lambda(h)$ / U_S *vs.* Θ relation	λ_0	$\frac{\lambda_1}{h}$	$\frac{\lambda_2}{h^2}$
Linear	$h_{rrr}\|_{r=R(t)} = 2318$ (singular) Time to spread: $t = 10.3$	$h_{rrr}\|_{r=R(t)} = 3.15$ Time to spread: $t = 4.5$	$h_{rrr}\|_{r=R(t)} = -0.10$ Time to spread: $t = 3.9$
Quadratic	$h_{rrr}\|_{r=R(t)} = 771$ (singular) Time to spread: $t = 14.3$	$h_{rrr}\|_{r=R(t)} = 1.60$ Time to spread: $t = 7.2$	$h_{rrr}\|_{r=R(t)} = -0.055$ Time to spread: $t = 5.9$
Cubic	$h_{rrr}\|_{r=R(t)} = 390$ (singular) Time to spread: $t = 20.0$	$h_{rrr}\|_{r=R(t)} = 0.87$ Time to spread: $t = 11.0$	$h_{rrr}\|_{r=R(t)} = -0.029$ Time to spread: $t = 9.1$

TABLE 2. Contrasting third derivatives and spreading times for the various numerical schemes. The various cases are allowed to spread until the drop radius reaches a size of 1.25. The values of the third derivative of h at the contact line $r = R(t)$, and the times necessary to reach that size are then tabulated

Finally, we summarize the numerical results of this section in table 2. There we give for each of the three slip coefficients (1.2) and each of the three slip velocity–contact angle relationships (2.11) the value of the third derivative at the contact line when the radius has spread to $R = 1.25$, and the time taken to spread that far. The third derivative is calculated by evaluating the pseudo-spectral approximation at the contact line. In our numerical method the differential equation is never imposed at the contact line so possible singularities at the contact line are avoided in the calculation. The singular-slip-coefficient cases both have finite third

derivatives at the contact line. We see from table 2 that the magnitude of this derivative is at least an order of magnitude larger in the λ_1 case than in the λ_2 case. As noted in the local analysis of §3 the third derivative will be singular in the constant-slip-coefficient case. The values for the derivatives reported in that column should be taken as an indicator of the strength of the singularity. That the code does try to capture this singularity can be demonstrated by examining the third derivative with increasing number of modes, N. For example, in the linear case with $N = 16$, 32 and 64, the third derivative at the contact line has the values of 439, 2318 and 10423 respectively. Even with this singularity, the height h, its first derivative and the drop radius R show a convergence along all of the drop. The next comparisons in table 2 are the spreading rates. We first note that the rate of spreading increases as the singularity in the slip coefficient increases. Also, for the cases considered here, we find that the spreading rate increases as we move from the cubic to the quadratic to the linear slip velocity–contact angle relationships. As shown in figure 9 this is not in general true but depends on the initial data, but as noted earlier the trend is true for large times. We have set $N = 32$ for the results presented in table 2.

5. Conclusions

The motion of a viscous droplet has been determined using the lubrication model (2.12), (2.20)–(2.26). We have considered several slip coefficients and slip velocity–contact angle relationships. These models were solved asymptotically for short time and numerically for finite time using a pseudo-spectral method. We find that the spreading rates strongly depend on the form of these relationships but the qualitative features of the droplet motion are similar in all cases.

We have chosen to consider slip coefficients that were either a constant or inversely proportional to the droplet thickness, or its square. The slip velocity–contact angle relationships chosen were either for constant angle or for the slip velocity proportional to the difference of the contact angle from its static value, or proportional to the square or cube of these differences. These relationships were chosen here but the proper form of the relationship should be determined by an analysis in the neighbourhood of the contact line. There has been some work in this direction (Hocking 1977; Jansons 1986), but many questions still remain. Our results and those of Dussan V. (1976) for small capillary number imply that although the qualitative features of the motion are similar in all cases, in order to compare with experimental data specific features of the model are required. On the other hand, using the results presented here and comparing with experimental data it could now be possible to choose a model. If data on the spreading rates of a droplet and slip velocity–contact angle relationship were found, one could determine which of the models (1.2) and (2.11) best fit the data. Once this is done specific predictions, such as the dissipation associated with the contact-line motion, could be made. Finally, we note that other models of contact-line motion different from those presented here could be solved by our method.

The authors wish to thank Alvin Bayliss and Steve Davis for several helpful discussions. This work was supported in part by DOE Grant No. DE-FG02-88ER13927. Also, acknowledgement is made to the Donors of the Petroleum Research Fund administered by the American Chemical Society for partial support of this research.

REFERENCES

CANUTO, C., HUSSAINI, M. Y., QUARTERONI, A. & ZANG, T. A. 1988 *Spectral Methods in Fluid Dynamics*. Springer.

CHEN, J. 1988 Experiments on a spreading drop and its contact angle on a solid. *J. Colloid Interface Sci.* **122**, 60–72.

DAVIS, S. H. 1980 Moving contact lines and rivulet instabilities. Part 1. The static rivulet. *J. Fluid Mech.* **98**, 225–242.

DAVIS, S. H. 1983 Contact-line problems in fluid mechanics. *Trans. ASME* E: *J. Appl. Mech.* **50**, 977–982.

DUSSAN V., E. B. 1976 The moving contact line: the slip boundary condition. *J. Fluid Mech.* **77**, 665–684.

DUSSAN V., E. B. 1979 On the spreading of liquids on solid surfaces: Static and dynamic contact lines. *Ann. Rev. Fluid Mech.* **11**, 371–400.

DUSSAN V., E. B. & DAVIS, S. H. 1974 On the motion of a fluid–fluid interface along a solid surface. *J. Fluid Mech.* **65**, 71–95.

EHRHARD, P. & DAVIS, S. H. 1990 Non-isothermal spreading of liquid drops on horizontal plates. *Applied Mathematics Tech. Rep.* 8920. Northwestern University, Evanston, IL.

GENNES, P. G. DE 1985 Wetting: statics and dynamics. *Rev. Mod. Phys.* **57**, 827–863.

GOTTLIEB, D. & ORSZAG, S. A. 1977 *Numerical Analysis of Spectral Methods: Theory and Applications*. CBMS-NSF Regional Conference Series in Applied Mathematics, Vol. 26, SIAM.

GREENSPAN, H. P. 1978 On the motion of a small viscous droplet that wets a surface. *J. Fluid Mech.* **84**, 125–143.

GREENSPAN, H. P. & MCCAY, B. M. 1981 On the wetting of a surface by a very viscous fluid. *Stud. Appl. Maths* **64**, 95–112.

HALEY, P. J. 1990 A numerical investigation of contact line motion. Thesis, Department of Applied Mathematics, Northwestern University, Evanston, IL.

HOCKING, L. M. 1977 A moving fluid interface. Part 2. The removal of the force singularity by a slip flow. *J. Fluid Mech.* **77**, 209–229.

HOCKING, L. M. 1981 Sliding and spreading of thin two-dimensional drops. *Q. J. Mech. Appl. Maths* **34**, 37–55.

HOCKING, L. M. 1983 The spreading of a thin drop by gravity and capillarity. *Q. J. Mech. Appl. Maths* **36**, 55–69.

HOCKING, L. M. & RIVERS, A. D. 1982 The spreading of a drop by capillary action. *J. Fluid Mech.* **121**, 425–442.

HOFFMAN, R. L. 1975 A study of the advancing interface. I. Interface shape in liquid-gas systems. *J. Colloid Interface Sci.* **50**, 228–241.

HUH, E. & MASON, S. G. 1977 The steady movement of a liquid meniscus in a capillary tube. *J. Fluid Mech.* **81**, 401–419.

HUH, E. & SCRIVEN, L. E. 1971 Hydrodynamic model of steady movement of a solid/liquid/fluid contact line. *J. Colloid Interface Sci.* **35**, 85–101.

JANSONS, K. M. 1986 Moving contact lines at non-zero capillary number. *J. Fluid Mech.* **167**, 393–407.

JOHNSON, R. E., DETTRE, R. H. & BRANDRETH, D. A. 1977 Dynamic contact angles and contact angle hysteresis. *J. Colloid Interface Sci.* **62**, 205–212.

KOPLIK, J., BANAVAR, J. R. & WILLEMSEN, J. F. 1989 Molecular dynamics of a fluid flow at solid surfaces. *Phys. Fluids* A **1**, 781–794.

ROSENBLAT, S. & DAVIS, S. H. 1985 How do liquid drops spread on solids? In *Frontiers in Fluid Mechanics* (ed. S. H. Davis & J. L. Lumley), pp. 171–183. Springer.

STAROV, V. M. 1983 Spreading of droplets of nonvolatile liquids over a flat surface. *Colloid J. USSR* (English Transl.) **45**, 1009.

VAN DYKE, M. 1975 *Perturbation Methods in Fluid Mechanics*. Parabolic.

YOUNG, G. W. & DAVIS, S. H. 1987 A plate oscillating across a liquid interface: effects of contact-angle hysteresis. *J. Fluid Mech.* **174**, 327–356.